Atmospheric
Measurement
Techniques
Open Access
Discussions

Mirror contamination in space I: approach

J. M. Krijger[1], R. Snel[1], G. van Harten[2], J. H. H. Rietjens[1], and I. Aben[1]

[1]SRON Netherlands Institute for Space Research, Sorbonnelaan 2, 3584CA Utrecht, the Netherlands
[2]Leiden Observatory, Leiden University, Niels Bohrweg 2, 2333CA Leiden, the Netherlands

Correspondence to: J. M. Krijger (krijger@sron.nl)

| Discussion Paper | | Discussion Paper | | Discussion Paper | | Discussion Paper |

AMTD

7, 1213–1246, 2014

Mirror contamination I

J. M. Krijger et al.

Title Page

Abstract	Introduction
Conclusions	References
Tables	Figures

|◄ | ►|
◄ | ►

Back | Close

Full Screen / Esc

Printer-friendly Version

Interactive Discussion

Abstract

We present a comprehensive model that can be employed to describe and correct for degradation of (scan) mirrors and diffusers in satellite instruments that suffer from changing optical UV-VIS properties during their operational lifetime. As trend studies become more important, so does the importance to understand and correct for this degradation. This is the case not only with respect to the transmission of the optical components, but also with respect to wavelength, polarisation or scan-angle-effects. Our hypothesis is that mirrors in-flight suffer from the deposition of a thin absorbing layer of contaminant, which slowly builds up over time. We describe this with the Mueller matrix formalism and Fresnel equations for thin multi-layer contamination films. Special care is taken to avoid the confusion often present in earlier publications concerning Mueller matrix calculus with out of plane reflections. The method can be applied to any UV-VIS satellite instrument, and in any orbit, both low and geostationary. We illustrate and verify our approach on the optical behaviour of the multiple scan mirrors of SCIAMACHY (on board of ENVISAT).

1 Introduction

Almost all optical instruments in space suffer from transmission loss due to in-flight degradation of optical components and/or detectors. This transmission loss, especially at the shorter UV wavelengths can, in worst case, cause a nearly complete loss of detectable photons, and in lesser cases a strong decrease in the signal-to-noise ratio. Often this transmission loss is corrected by solar calibration, e.g., using a diffuser to observe the (assumed stable) sun. However, instruments employing scan mirrors often observe their scientific targets under different angles than their (in-flight) calibration sources. As more satellites spend longer time in orbit it became clear that the transmission loss or degradation is dependent on the scan angle (of the scan mirror) (Krijger et al., 2005b; Tilstra et al., 2012). This has been referred to as the

scan-angle-dependent-degradation. This problem is becoming more pressing with the increasing number of long-term (climate) trends studies.

Our hypothesis is that both scan mirrors and surface diffusers suffer from a thin absorbing layer of contaminant, which slowly builds up over time. Many previous studies into such contaminant layers that form on mirrors and/or diffusers in space have been performed. However due to their technical nature many did not appear into the peer-reviewed scientific journals. Studies like, e.g., the one of Stiegman et al. (1993) on diffusers show some organic effluent present, but did not allow for the identification of the contaminant. Also Chommeloux et al. (1998) showed the on-ground degradation as a result of UV- or photon-radiation, as did Georgiev and Butler (2007) or Fuqua et al. (2004). In-flight studies of contaminant are of course more difficult. Some studies are collected in an extensive database, which has been made recently available to the general public (Green, 2001). In summary most of the early satellites suffered from degradation caused by outgassing. However the exact identity of the contaminant causing the UV-VIS degradation remained unclear. McMullin et al. (2002) studied the degradation of SOHO/SEM and found they could explain the degradation with a thin layer of carbon forming on the forward aluminium filter. The exact source of the contaminant is unknown but suspected to be outgassing of the satellite itself. Schläppi et al. (2010) have attempted in situ mass spectrometry with ROSETTA to measure the constituents of their contamination and found the main contaminants to be water. In addition organics from the spacecraft structure, electronics and insulations were identified. Water was also found in SCIAMACHY, where it was deposited on the cold detectors (Lichtenberg et al., 2006). In fact, earth observing satellites suffer from degradation, both in throughput, and in the polarisation and/or scan-angle dependence, such as GOME (Krijger et al., 2005a; Slijkhuis et al., 2006), MODIS (Xiong et al., 2003; Xiong and Barnes, 2006; Meister and Franz, 2011), SeaWiFs (Eplee et al., 2007), VIIRS (Lei et al., 2012), MERIS (Delwart, 2010), SCIAMACHY (Bramstedt et al., 2009)[1] and the two GOME-2

---

[1]data at: http://www.iup.uni-bremen.de/sciamachy/mfactors/

(Lang, 2012) instruments currently in orbit. Most provide an empiric degradation correction for the data users.

Thin layer deposits on mirrors and diffuser has been modelled before (e.g., most recently by Lei et al., 2012), however these earlier attempts focus only on transmission loss and often do not take scan-angle-dependence into account and none consider polarisation. These, however, need to be considered for a proper description of in-flight behaviour. This can be done employing the Mueller matrix formalism and Fresnel equations. The application of Mueller matrix calculation in combination with the Fresnel equations requires special care due to their different mathematical descriptions of polarized light, especially in case of out of plane reflections. However there are many ambiguities in often not well defined absolute polarisation-frames, in the direction or handedness in the often ignored circular polarisation, in naming conventions, or in the application of signs with respect to frame-changes, which often lead to much confusion. Therefore in this paper we go for the first time[2] into full detail and present a consistent, well defined approach for Mueller matrix calculation in combination with Fresnel equations, using detailed illustrations and descriptions to describe the mathematics and frames. We will show that this approach is in full agreement with verification measurements and generally applicable.

This study was initiated to investigate the wavelength and scan-angle-dependent degradation as observed by SCIAMACHY, on-board ENVISAT (Gottwald and Bovensmann, 2011), which affects long term data records. So the optical behaviour of the scan mirror of SCIAMACHY has been simulated based on this model and was compared with measurements during on-ground calibration and dedicated laboratory measurements, which shows that the model performs very satisfactorily under those early on-ground conditions. Application and analyses of in-flight (SCIAMACHY) contaminations and its behaviour over time will be presented in a follow-up paper in this series.

---

[2]to the authors knowledge

The great value of this model is that it is generally applicable and can be easily applied to all satellites, both in low and geostationary orbit, employing (scan) mirrors or other optics suffering from degradation due to contamination. This includes the even more simpler cases where either only wavelength dependent or scan-angle-dependent degradation is observed. The model can provide detailed scan-angle and wavelength behaviour as a function of time, allowing for accurate correction, which is needed for precise (trend) analyses.

In Sect. 2 we describe a model for a scan mirror and a surface diffuser. In Sect. 3 we shortly describe SCIAMACHY, important for our verification. This verification using on-ground measurements is described in Sect. 4. A general discussion follows. Finally we will conclude on the model with an outlook to its application.

2 Model

2.1 Mueller calculus

In order to model the scan-angle dependent throughput of mirrors we employ the well-known Stokes and Mueller calculus (Azzam and Bashara, 1987; Hecht and Zajac, 1974). The incoming (partly) polarised light is characterized by a Stokes vector I

$$I = \begin{pmatrix} I \\ Q \\ U \\ V \end{pmatrix} \tag{1}$$

Here, I is the intensity, Q and U describe the two-dimensional state of linear polarisation, and V represents circular polarisation.

Any description of polarisation requires an exact reference frame definition. In this paper we use the same reference frame and conventions as Hecht and Zajac (1974). This means that when looking along the direction the light is travelling, positive U is

Mirror contamination I

J. M. Krijger et al.

found by rotating 45° counter-clockwise from Q, while positive V is defined when the E vector is rotating clockwise, as shown in Fig. 1. Note that the rotation and direction of the E vector is defined in a fixed reference frame or plane. Many other frame definitions are in use, however these will require different Mueller matrices than used in this text.

Often the Stokes vector I is split in a total signal part and polarisation vector,

$$I = I_0 \cdot \begin{pmatrix} 1 \\ q \\ u \\ v \end{pmatrix} \qquad (2)$$

with q, u, and v, the fractional polarisation Q, U, and V with respect to the total signal, I_0.

Any detected signal S depends on the received polarised light I and the polarisation-sensitivity of the instrument μ,

$$S = \mu \cdot I \qquad (3)$$

with

$$\mu = M_1 \cdot (1, \mu_2, \mu_3, \mu_4) \qquad (4)$$

with M_1 the absolute radiance sensitivity of the instrument and μ_x the normalised polarisation-sensitivity of q, u, and v of the instrument, respectively.

Any optical element that modifies the polarised light, such as retarders, polarizers, mirrors, can be described as a 4×4 transformation matrix M (known as the Mueller matrix):

$$S = \mu \cdot M \cdot I \qquad (5)$$

For polarisation-insensitive detectors often the first row of M is considered equivalent to μ, thus removing the need for μ. However here we consider a possible polarisation-sensitive instrument and choose to employ μ explicitly.

Multiple elements encountered by the light can be described by multiplying consecutive Mueller matrices:

$$S = \boldsymbol{\mu} \cdot \mathbf{M}_n....\mathbf{M}_3\mathbf{M}_2\mathbf{M}_1 \cdot \boldsymbol{I} \tag{6}$$

Note that for Mueller matrix calculations the first encountered element by the light is the one farthest right in the formula. Matrix multiplication is not commutative, so order is important.

It is always important to define the reference frame both at the detector and at the source, and to keep track of the frame at different position between source and detector, since a frame rotation might be needed between two optical components when out-of-plane reflections happen. In reflections often the p and s directions are used. The p polarisation (p from parallel) is the polarisation in the plane of reflection or incidence, while s polarisation (s from senkrecht, German for perpendicular) is perpendicular to this plane (See Fig. 2). The p and s frame can be, and often is coupled, to a Stokes frame in case of a single reflection, with $S \equiv Q = 1$ and $P \equiv Q = -1$. However this is a choice and can be different, as long as the Stokes frame is rotated before and after a reflection to the p and s frame (see Sect. 2.5 for more details on frame rotations). For example the mirror in Fig. 2 would have to be rotated 90° in order to match the frame from Fig. 1 with $S \equiv Q = 1$.

2.2 Mirror model

The generic Mueller matrix for a mirror, defined in the reference frame of Fig. 1, with angle of incidence of the light given by ϕ_{mir} and plane of reflection perpendicular to the $Q = 1$ direction is given by Azzam and Bashara (1987):

$$\mathbf{M}_{\mathrm{mir}}(\phi_{\mathrm{mir}}) = \begin{pmatrix} \frac{1}{2}(r_s^2 + r_p^2) & \frac{1}{2}(r_s^2 - r_p^2) & 0 & 0 \\ \frac{1}{2}(r_s^2 - r_p^2) & \frac{1}{2}(r_s^2 + r_p^2) & 0 & 0 \\ 0 & 0 & |r_p||r_s|\cos(\Delta) & |r_p||r_s|\sin(\Delta) \\ 0 & 0 & -|r_p||r_s|\sin(\Delta) & |r_p||r_s|\cos(\Delta) \end{pmatrix} \tag{7}$$

where the complex reflection coefficients r_p and r_s for s and p polarised light are given by the Fresnel equations:

$$r_p = \frac{n_2 \cos(\phi_{mir}) - n_1 \sqrt{1 - \left(\frac{n_1}{n_2} \sin(\phi_{mir})\right)^2}}{n_2 \cos(\phi_{mir}) + n_1 \sqrt{1 - \left(\frac{n_1}{n_2} \sin(\phi_{mir})\right)^2}} \tag{8}$$

$$r_s = \frac{n_1 \cos(\phi_{mir}) - n_2 \sqrt{1 - \left(\frac{n_1}{n_2} \sin(\phi_{mir})\right)^2}}{n_1 \cos(\phi_{mir}) + n_2 \sqrt{1 - \left(\frac{n_1}{n_2} \sin(\phi_{mir})\right)^2}} \tag{9}$$

The complex indices of refraction of the mirror material and ambient medium are denoted by n_2 and n_1. Note $n = n_r - ik$, with $k \geq 0$, with n_r the real part and k the imaginary part. This makes k a damping factor, which describes the absorption of light by metals (see van Harten et al., 2009). Note that the s and p direction are given here according to the conventional definition, with p in the plane of reflection and s perpendicular to this plane. The phase jump Δ in this coordinate frame is defined as:

$$\Delta = \arg(r_p) - \arg(r_s) \tag{10}$$

On a side note: a perfect reflection is described by:

$$\mathbf{M}_{\text{perfect reflection}} = \tag{11}$$

$$\begin{pmatrix} 1 & 0 & 0 & 0 \\ 0 & 1 & 0 & 0 \\ 0 & 0 & -1 & 0 \\ 0 & 0 & 0 & -1 \end{pmatrix}$$

The reflection Mueller matrix correctly describes that the signs of U and V flip. This is a direct consequence of the fact that the Stokes frame is defined for an observer

looking along the beam, so upon reflection the definitions of left and right are swapped. This sign-change of U and V can be mathematically achieved by changing the signs in the lower-right quadrant of the mirror Mueller matrix (e.g., see Keller, 2002) or as was done here by the definition of Δ with r_p and r_s, which cause a 180° phase difference for a perfect reflection.

2.3 Diffuser model

The mirror model can also be employed to describe the behaviour of a surface diffuser. The roughened surface contains many irregularities (or facets) which causes light to be reflected in various directions, thus decreasing the transmission in the direction of the instrument. The assumption here is made that for polarisation behaviour the diffuser can be considered as a large number of small mirror facets. Only those facets contribute to the signal which are oriented such that they cause specular reflection of the light into the direction of the instrument (see Fig. 3). Thus the geometry dictates the relative polarisation behaviour, while the unpolarised reflectivity is only a function of the angular distribution of the facets of the diffuser, and the orientation of the diffuser in the light path. The Mueller matrix for a surface diffuser is then given by:

$$\mathbf{M}_{dif}(\phi_{in}, \phi_{out}) = M_1^{dif}(\phi_{in}, \phi_{out}) \cdot \mathbf{M}_{mir}(\phi_{dif}), \tag{12}$$

with the scalar M_1^{dif} the diffuser sensitivity and

$$\phi_{dif} = \frac{1}{2}(\phi_{in} + \phi_{out}) \tag{13}$$

with ϕ_{in} and ϕ_{out} both positive angles with respect to the normal, and $\mathbf{M}_{mir}$ as in Eq. (7). Figure 3 shows the various angles.

2.4 Contamination

Our hypothesis is that degrading mirrors and diffusers degrade through deposition of thin absorbing layers of contaminant, which change over time. Thus the model was

extended to allow up to 2 layers with specified thickness and refractive index (Azzam and Bashara, 1987; Born and Wolf, 1999). The change to the model as presented in Sect. 2.2, is only in the equations for the reflection coefficients r_s and r_p, combined here as an implied s and p specific reflection coefficient r_t. Note that this is a different approach from that described in van Harten et al. (2009), as we include each extra layer explicitly. The total reflection coefficient for the bulk or substrate (subscript 4) with refractive index n_4, the first layer (subscript 3) with refractive index n_3, the second layer (subscript 2) with refractive index n_2 and the ambient medium (subscript 1) with refractive index n_1 combined is given by (see also Fig. 4 for a graphical explanation):

$$r_t = \frac{r_{12} + R_{23}e^{(-2i\delta_2)}}{1 + r_{12}R_{23}e^{(-2i\delta_2)}} \tag{14}$$

where r_{jk} are the r_s and r_p reflection coefficients between media with subscripts j and k as given by Eqs. (8) and (9), and

$$R_{23} = \frac{r_{23} + r_{34}e^{(-2i\delta_3)}}{1 + r_{23}r_{34}e^{(-2i\delta_3)}} \tag{15}$$

$$\delta_2 = 2\pi\frac{d_2}{\lambda}n_2\cos(\phi_2) \tag{16}$$

$$\cos(\phi_2) = \sqrt{1 - \left(\frac{n_1}{n_2}\sin(\theta)\right)^2} \tag{17}$$

$$\delta_3 = 2\pi\frac{d_3}{\lambda}n_3\cos(\phi_3) \tag{18}$$

$$\cos(\phi_3) = \sqrt{1 - \left(\frac{n_1}{n_3}\sin(\phi_1)\right)^2} \tag{19}$$

with ϕ_x the angle of incidence in medium x (only ϕ_1 is needed, the other can be derived as shown), λ the wavelength of the light, and d_2 and d_3 the layer thicknesses of the layer closest to the ambient medium and the substrate, respectively.

2.5 Multiple mirrors

Some instruments, such as SCIAMACHY, employ multiple scan mirrors. As a result both polarisation and throughput changes as a function of the viewing angle of each mirror. The modelling of the reflection from multiple mirrors may require the use of rotation matrices. Especially in cases where the planes of two successive reflections are not parallel, a rotation of the reference frame is needed in order to align the $Q = 1$ direction of the reference frame with the s direction corresponding to the plane of reflection. The rotation matrix over an arbitrary angle γ is given by:

$$\mathbf{R}(\gamma) = \begin{pmatrix} 1 & 0 & 0 & 0 \\ 0 & \cos(2\gamma) & -\sin(2\gamma) & 0 \\ 0 & \sin(2\gamma) & \cos(2\gamma) & 0 \\ 0 & 0 & 0 & 1 \end{pmatrix} \tag{20}$$

Using this Mueller matrix with $\gamma = 45°$ changes $Q = 1$ into $U = 1$. In order to add an optical element with Mueller matrix $\mathbf{M}$ placed under an angle γ, one has to mathematically rotate the element in line as follows, to get it to align with our frame:

$$\mathbf{M}_{\text{rot}} = \mathbf{R}(\gamma) \cdot \mathbf{M} \cdot \mathbf{R}(-\gamma) \tag{21}$$

For a mirror, where the reflection flips the coordinates, the back transformation should hence also be mirrored (Keller, 2002), resulting in:

$$\mathbf{M}_{\text{rot}} = \mathbf{R}(-\gamma) \cdot \mathbf{M} \cdot \mathbf{R}(-\gamma) \tag{22}$$

For clarity note that all rotation signs can be swapped as long as they are then also changed in the rotation matrix. Sometimes both definitions are used in the same book,

Title Page

Abstract | Introduction

Conclusions | References

Tables | Figures

|◀ | ▶|

◀ | ▶

Back | Close

Full Screen / Esc

Printer-friendly Version

Interactive Discussion

e.g. in Azzam and Bashara (1987). Note that for polarisation two positive rotation does not equal two negative rotations due to handedness of polarisation.

Combining the two mirrors can then be written as:

$$\mathbf{M}_{mir}(\phi_{mir1}, \phi_{mir2}) = \mathbf{R}(-\gamma_{mir2}) \cdot \mathbf{M}(\phi_{mir2}) \cdot \mathbf{R}(-\gamma_{mir2}) \cdot \mathbf{R}(-\gamma_{mir1}) \cdot \mathbf{M}(\phi_{mir1}) \cdot \mathbf{R}(-\gamma_{mir1}) \quad (23)$$

Each rotation is with respect to the initial Stokes-frame of the light incident on the optical element. This allows changing from e.g. an external frame to an instrument frame and vice-versa by adding the appropriate rotation matrix. When employing two mirrors the angle of incidence on the second mirror depends on the angles under which the mirrors are rotated with respect to each other. An example of modelling two mirrors applied to the case of SCIAMACHY will be shown in the next section.

3 SCIAMACHY

The SCIAMACHY (Gottwald et al., 2006) calibration concept (Noël et al., 2003) builds on a combination of on-ground and in-flight calibration measurements. The on-ground calibration measurements were split up into ambient measurements comprising the scanner unit only, and thermal vacuum (TV) measurements using the entire instrument. Viewing angle dependence for the on-ground calibration data is derived from the ambient measurements, while the remainder of the calibration information is derived from the TV measurements. For in-flight conditions the combination of ambient and TV data is essential.

Unforeseen instrumental polarisation behaviour, most likely caused by thermally induced stress birefringence of one of the optical components in the instrument (Snel, 2000), required the initial calibration approach to be extended with additional on-ground polarisation characterisation of the instrument.

Shortly after launch discrepancies between the observed and expected signals were observed, and subsequently significantly reduced by means of ad hoc sign changes of selected polarisation calibration parameters. This solution was considered acceptable

Full Screen / Esc

Printer-friendly Version

Interactive Discussion

for the time being, and worked well for nadir viewing geometry but needed additional workarounds for limb geometry. Here however we will now employ a more fundamental approach. Our method is consistent in both nadir and limb, as we describe the various mirrors now in the same frame.

3.1 SCIAMACHY mirrors

Aluminum mirrors are known to induce instrumental polarization, when used at non-normal incidence (e.g. Thiessen and Broglia, 1959). Such mirrors however are often used in telescope mirrors, as on board SCIAMACHY. This phenomenon is caused by differential reflection between polarization in the plane of incidence and polarization perpendicular to it, as described by the Fresnel equations. The amount of polarization depends on the mirror material, angle of incidence and wavelength. For instance, reflection off an aluminum mirror at 45° turns unpolarized visible light into 3 to 4% polarization perpendicular to the plane of incidence (van Harten et al., 2009).

It has been shown that these polarization properties can not be described using the Fresnel equations for bare aluminum (Burge and Bennett, 1964). Attempts to fit measured instrumental polarization to an aluminum model lead to unrealistic pseudo-indices of refraction (Sankarasubramanian et al., 1999; Joos et al., 2008).

Indeed, this bare aluminum model is incomplete, since the instant an aluminum mirror is exposed to air, a few nanometers thick aluminum-oxide layer starts growing on its surface. This phenomenon, as explained theoretically by Mott (1939), has been measured using microscopy and spectroscopy by Jeurgens et al. (2002). Mueller matrix ellipsometry by van Harten et al. (2009) showed that the mirror polarization can be described by a $\sim 4.12 \pm 0.08$ nm aluminumoxide layer on top of bulk aluminum, where the layer grows asymptotically to the final thickness within the first ~ 10 days. This is also needed to adequately describe the aluminum mirrors in SCIAMACHY.

3.2 SCIAMACHY geometry

The SCIAMACHY scanner (Fig. 5) consists of two mechanisms, each containing a mirror with a diffuser on the back. The elevation scan mirror (ESM) is needed for all measurement modes and contains the main diffuser. The azimuth scan mirror (ASM) is only used in limb measurement mode, including sun over ESM diffuser mode. The ESM and ASM can be set at any angle.

SCIAMACHY has a geometry where detector and both mirrors are in the same plane but with perpendicular rotation axis (see Fig. 5). Let α_x be the rotation of mirror x among its axis, with 45° mirror rotation resulting in the light being reflected under 90°. For the ESM (employed for both nadir and limb scans) the angle of incidence towards the detector is equal to the rotation of the ESM on it's axis:

$$\phi_{ESM} = \alpha_{ESM} \tag{24}$$

When choosing the Stokes reference frames optimally (namely $S \equiv Q = 1$ for the ESM) the nadir case is very simple:

$$\mathbf{M}_{nadir}^{opt} = \mathbf{M}(\phi_{ESM}) \tag{25}$$

For limb observations the situation is a bit more complicated, because one has to account for the different orientation of the planes of reflection of the ESM and ASM with respect to the Stokes reference frames of the incoming and outgoing light. The rotation angle between the plane of reflection of the ESM and the ASM is given by:

$$\gamma_{ASM \rightarrow ESM} = \pi/2 + \arcsin(\cot(\phi_{mir1}) \cdot \tan(2\phi_{mir2})) \tag{26}$$

Also the ASM must be placed under a very specific angle in order to reflect the light onto the ESM and then the detector/instrument slit. The required angle of incidence on the ASM can be calculated using:

$$\phi_{ASM} = \arccos(\cos(\alpha_{ASM}) \cdot \cos(2\alpha_{ESM})) \tag{27}$$

The total Mueller matrix for limb observations is then given by

$$\mathbf{M}_{\text{limb}}^{\text{opt}} = \mathbf{M}(\phi_{\text{ESM}}) \cdot \mathbf{R}(-\gamma_{\text{ASM}\rightarrow\text{ESM}}) \cdot \mathbf{M}(\phi_{\text{ASM}}) \cdot \mathbf{R}(-\gamma_{\text{ASM}\rightarrow\text{ESM}}) \quad (28)$$

However, for historical reasons, the $Q = 1$ direction was chosen perpendicular to the entrance slit of SCIAMACHY, see Fig. 5, i.e. parallel to the scattering plane of the ESM, or 90° compared to the simple case. This requires several rotations, resulting in a Mueller matrix for nadir observations:

$$\mathbf{M}_{\text{nadir}}^{\text{hist}} = \mathbf{R}(-\gamma_{\text{ESM}}) \cdot \mathbf{M}(\phi_{\text{ESM}}) \cdot \mathbf{R}(-\gamma_{\text{ESM}}) \quad (29)$$

with $\gamma_{\text{ESM}} = 90°$.

The total Mueller matrix for limb observations can be derived by a frame-rotation for each mirror element and is then given by

$$\mathbf{M}_{\text{limb}}^{\text{hist}} = \mathbf{R}(-\gamma_{\text{ESM}}) \cdot \mathbf{M}(\phi_{\text{ESM}}) \cdot \mathbf{R}(-\gamma_{\text{ESM}}) \cdot \mathbf{R}(-\gamma_{\text{ESM}})$$
$$\cdot \mathbf{R}(-\gamma_{\text{ASM}\rightarrow\text{ESM}}) \cdot \mathbf{M}(\phi_{\text{ASM}}) \cdot \mathbf{R}(-\gamma_{\text{ASM}\rightarrow\text{ESM}}) \cdot \mathbf{R}(-\gamma_{\text{ESM}}) \quad (30)$$

As rotations are commutative, and two 90° rotations equal a full rotation for polarisation, this equation can be simplified here to:

$$\mathbf{M}_{\text{limb}}^{\text{hist}} = \mathbf{R}(-\gamma_{\text{ESM}}) \cdot \mathbf{M}(\phi_{\text{ESM}}) \cdot \mathbf{R}(-\gamma_{\text{ESM}}) \cdot \mathbf{R}(-\gamma_{\text{ASM}}) \cdot \mathbf{M}(\phi_{\text{ASM}}) \cdot \mathbf{R}(-\gamma_{\text{ASM}}) \quad (31)$$

with,

$$\gamma_{\text{ASM}} = \arcsin(\cot(\phi_{\text{mir1}}) \cdot \tan(2\phi_{\text{mir2}})) \quad (32)$$

Finally, we emphasise that these formulas will change if different Stokes reference frames are used, but the approach remains the same.

Mirror contamination I

J. M. Krijger et al.

Title Page

Abstract	Introduction
Conclusions	References
Tables	Figures

◄ | ►►

◄ | ►

| Back | Close |

Full Screen / Esc

Printer-friendly Version

Interactive Discussion

4   Verification

Combining Mueller matrix formalism with the Fresnel equations requires, especially in the case of out-of-plane reflections, a precise definition and bookkeeping of mathematical signs and conventions. In particular, this applies to the absolute polarisation frame, to the rotations between frames before and after reflection, to the handedness of circularly polarised light, and to the implementation in the form of an algorithm.

Hence it is of the utmost importance to verify Mueller matrix calculations. In this section, we apply our model to SCIAMACHY on-ground measurements of the diffuser and scan mirrors. We show that all data can be well explained using Mueller matrix calculations in combination with the Fresnel equations, confirming the correct use of these tools.

4.1   Refractive index

In the section below we compare model calculations with older on-ground measurements performed on aluminum mirrors during SCIAMACHY calibration. As mentioned, these aluminum mirrors were not vacuum protected and will thus have a thin layer of aluminum oxide on them. In order to describe these mirrors, the refractive index of aluminum and aluminum-oxide is needed for the wavelength range of interest (here 300–2400 nm). However there are several conflicting aluminum refractive indices available in literature (likely due to the way they deal with the aluminum oxide layer), namely the direct measurements found in Haynes (2013) and Palik (1985) and the Kramers-Kronig-derived values of Rakic (1995). While the differences in refractive index can be several percent, the difference in specific applications is much harder to quantify. Our verification results improved very slightly when employing the indices of Rakic (1995) and hence the choice was made to employ these indices.

To the best of our knowledge, in literature there is no complete information on the refractive index of amorphous aluminum-oxide in the 0.2–2.4 μm wavelength range.

However the work of Edlou et al. (1993) can be extrapolated by using the Cauchy dispersion equation:

$$n(\lambda) = A + B\lambda^{-2} + C\lambda^{-4} \tag{33}$$

to the desired wavelength range. We employ the values found by Edlou et al. (1993) of $1.63, 2.25 \times 10^3\,\text{nm}^2, 20.16 \times 10^7\,\text{nm}^4$ for A, B and C, respectively. This latter option was employed for its ability to interpolate accurately to desired wavelengths.

4.2 Mirror model verification

First we compared the mirror model with the measurements of van Harten et al. (2009). Shown in Fig. 6 is the comparison at 600 nm, using a refractive index for aluminium of $1.262 - i7.186$ and an refractive index for the aliminium oxide, calculated by Eq. (33), of $1.637 - i0.000$ at the measured wavelength of 600 nm, for the different Mueller Matrix components. The normalised, to the top-left element, measurements are assumed to be accurate within 0.02. The first column components, the instrumental polarisation sensitivity here, has residuals smaller than 0.003 and are thus in almost perfect agreement. The diagonal components, indicating the transmission of polarization, have residuals smaller than 0.01. Other (polarisation cross-talk) residuals remain below 0.02, but here the measurements might have suffered from limited calibration accuracy (For more discussion on the measurements, see van Harten et al. (2009)). In summary, the residuals between measurement and model are within the measurement accuracy, hence the measurement data and model are in excellent agreement.

For another verification we turned to SCIAMACHY. During on-ground calibration SCIAMACHY's aluminium scan mirrors reflectivity was measured with different polarisation-orientations of the incoming light, both with single and multiple mirrors.

We show the most complicated situation first with multiple mirrors, where multiple orientations of linear polarisation ($Q = 1$, $Q = -1$, $U = 1$, and $U = -1$ with respect to the SCIAMACHY reference frame) were reflected on the whole scanner unit. The reflected light was then analysed employing linear polarisation filters (either $Q = 1$ or

Title Page

Abstract | Introduction

Conclusions | References

Tables | Figures

◀ | ▶

◀ | ▶

Back | Close

Full Screen / Esc

Printer-friendly Version

Interactive Discussion

$Q = -1$). Shown in Fig. 7 are both measurement and model simulations under the SCIAMACHY references viewing angles ($\phi_{ESM} = 12.7°$ and $\phi_{ASM} = 45°$) for the various combination of offered and measured polarisation directions. Original estimated errors bars are shown, however already during the measurements it was clear these were too optimistic (Dobber, 1999). But as can be seen, the measurements originally differed several standard deviations from a simple clean mirror model employing literature value for the refractive index of aluminium. Including a 4.12 nm layer of aluminium oxide (van Harten et al., 2009) improves the comparison significantly, however for the shortest wavelength an additional contamination was needed. A correction by increasing the thickness of the aluminium oxide to 9 nm (not shown) showed improvement but did not show the correct wavelength behaviour and was rejected. Further investigation showed that employing a 0.4 nm of light oil contamination on the surface of the mirror is needed in order to correctly model the measurements.

The light oil optical properties were taken from Barbaro et al. (1991). Such a small contamination of 0.4 nm on the mirror was within the molecular cleanliness control requirements (van Roermund, 1996) during on-ground measurements. Of course the exact kind of oil or even the kind of contaminant is unknown, however the assumption of light oil contamination is not unreasonable.

The good agreement between measurements and model clearly shows that the mirror model works very well, and that inclusion of aluminium oxide and oil contamination is necessary to explain the measurement results. Since an error or sign change in one of the rotation angles used in the calculation will result in completely different polarisation sensitivities (not shown here), Fig. 7 confirms that the correct signs and rotation angles are employed. The use of the optical properties of light oil, while the true contaminant source and its polarisation properties are as yet unknown, could be the reason for the differences at the shortest wavelengths. However more likely the measurements have larger uncertainties than originally stated.

The single mirror measurements are less sensitive to contaminations and are thus less useful for verification, but we show them here for completeness in Fig. 8. Again

Printer-friendly Version

Interactive Discussion

a 4.1 nm aluminum oxide and 0.4 nm light oil contamination were employed in order to employ identical mirrors as for the multiple mirror case. Measurement and model are in good agreement.

In order to verify the coordinate frames, verify employed Mueller matrices and avoid previous on-ground confusion, the authors have rebuilt the SCIAMACHY scanner setup in an optics lab. No new results where found, but all the measurements confirmed all rotations and Mueller matrices signs.

4.3 Diffuser model verification

The assumption that the diffuser acts as a surface diffuser with mirror facets can be checked by changing the angle of the mirror with respect to a fixed light source and fixed detector. In this case ϕ_{dif} is fixed, as the sum of the incident and outgoing angle, which is the angle between light source and instrument is fixed. Since $\mathbf{M}_{\mathrm{mir}}$ depends only on the fixed ϕ_{dif}, only the scalar $M_1^{\mathrm{dif}}(\phi_{\mathrm{in}}, \phi_{\mathrm{out}})$ will vary due to the change in the angle of incidence and outgoing angle (see Eq. 12). This will cause a change in the intensity of the signal, but not in the polarisation properties. Hence the relative polarisation should remain the same in this situation, irrespective of the angle with respect to the fixed light source and fixed detector.

A measurement to test this hypothesis has been performed on-ground for SCIA-MACHY. A scan over 40° rotation of the mirror was made, while keeping the light source and detector at a fixed position, over which a negligible change in polarisation was observed during the measurements. In Fig. 9 this is shown for a smaller range of rotation angles, near the operational rotation angle of 165°. In the figure the measured signal of the main science detectors for both s ($Q = 1$) and p polarisation ($Q = -1$) are plotted at 324 nm as a function of diffuser rotation angle. Both signals are scaled to the maximum of s polarisation for comparison, as the level of the signals is a scanner-independent instrument characteristic, depending on the instrument polarisation sensitivities. The signals show exactly the same response (within the error bars), as shown by their

plotted ratio, indicating that the polarisation did not change, only the total reflectance, as expected.

5 Discussion

We present here a method capable of describing the degradation as a function of both wavelength, polarisation and scan-angle for all earth observing instruments employing (scan) mirror in both low and geostationary orbits. In addition, employing a time-dependent contaminant layer thickness allows also to describe the degradation as function of time. Initially this work was started to solve the scan-angle-dependent-degradation of SCIAMACHY, but in this paper we have attempted to describe the method in the most generic way, for easy application to other instruments. Not all possible cases have been described, but expansion of the model to for example more mirrors or layers can be easily derived from the presented cases. The model is of interest to all instruments employing (scan) mirrors or other optics suffering from degradation due to contamination, including the simpler cases where no scan-angle-dependent-degradation but only wavelength-dependent degradation is present or vice versa. In its current version the model can provide detailed scan-angle and wavelength behaviour as a function of time, allowing for accurate correction, which is needed for precise (trend) analyses. We will further illustrate this by the application to SCIAMACHY in-flight measurements in the next paper in this series. Our current models allows up to two layers of contamination. The model is easily expanded with more layers, but for most applications a two layer model is sufficient which is described in detail here.

We have verified all assumptions and models and thus removed any remaining sign or frame inconsistencies. All formulae and verification results are fully consistent with each other. In previous measurements for e.g., SCIAMACHY (Gottwald and Bovensmann, 2011) different mirror configurations were taken as completely different measurements in sometimes conflicting or partially-defined polarisation frames. The current model always employs a well-defined frame with consistent mathematical

Mueller approach. All of these frame definitions and approaches have been used consistently for all verification measurements. With this approach we were able to describe all the measurements available to us. More proof of the correctness of the assumptions or approach employed will follow in a future paper in the series, where we will show the
5   model to also describe time-dependent in-flight measurement behaviour.

6   Conclusions

We have presented a model to accurately describe reflection and polarisation properties of multiple scan mirrors and diffusers in space. This model includes the impact of contamination, both spectrally and scan-angle-dependent. The model can be easily
10   applied to any satellite, both in low and geostationary orbit, employing (scan) mirrors or other optics suffering from degradation due contamination. Also in cases where no scan-angle-dependent-degradation but only wavelength-dependent degradation is present, the model allows for accurate in-flight corrections, provided information on the contamination can be constrained. Our hypothesis is that both scan mirrors and dif-
15   fusers suffer from a thin absorbing layer of contaminant, which slowly builds up over time. We described this transmission, polarisation and angle dependence of mirrors including multi-layers using the Mueller matrix formalism and Fresnel equations. In this paper we have gone into explicit detail, with respect to the handedness of the polarisation and mathematical signs accompanied by detailed illustrations and descriptions. We
20   resolve the long-standing ambiguities in the application of Mueller matrix and Fresnel calculations in (out-of-plane) reflections. As an application the SCIAMACHY scanner has been modelled based on this multiple layer contaminated mirror hypothesis. The model was checked against all known on-ground measurements, and shows excellent agreement under those conditions.
25   Looking to the future, the current model allows for up to two layers on the mirrors or diffuser, which will be used in a next paper in this series to investigate the

Back   Close

Full Screen / Esc

Printer-friendly Version

Interactive Discussion

observed UV-VIS signal loss over time and the scan angle dependent degradation of SCIAMACHY on-board ENVISAT.

References

Azzam, R., M., and Bashara, N.: Ellipsometry and Polarized Light, Elsevier, Amsterdam, NL, 1987. 1217, 1219, 1222, 1224

Barbaro, A., Mazzinghi, P., and Cecchi, G.: Oil UV extinction coefficient measurement using a standard spectrophotometer, Appl. Optics, 30, 852–857, doi:10.1364/AO.30.000852, 1991. 1230

Born, M. and Wolf, E.: Principles of Optics, Cambridge University Press, Cambridge, UK, 1999. 1222

Bramstedt, K., Noël, S., Bovensmann, H., Burrows, J., Lerot, C., Tilstra, L., Lichtenberg, G., Dehn, A., and Fehr, T.: SCIAMACHY monitoring factors: observation and end-to-end correction of instrument performance degradation, in: Atmospheric Science Conference, Vol. 676 of ESA Special Publication, 2009. 1215

Burge, D. K. and Bennett, H. E.: Effect of a thin surface film on the ellipsometric determination of optical constants, J. Opt. Soc. Am., 54, 1428–1433, 1964. 1225

Chommeloux, B., Baudin, G., Gourmelon, G., Bezy, J.-L., van Eijk-Olij, C., Schaarsberg, J. G., Werij, H. G., and Zoutman, E.: Spectralon diffusers used as in-flight optical calibration hardware, in: Society of Photo-Optical Instrumentation Engineers (SPIE) Conference Series, vol. 3427, edited by: Chen, P. T., McClintock, W. E., and Rottman, G. J., 382–393, 1998. 1215

Delwart, S.: Instrument Calibration Methods and Results, in: IOCCG Level 1 Workshop, Bathesda, 20–21 April, 2010. 1215

Dobber, M.: Ambient scan mirror and on-board diffuser calibration of the SCIAMACHY PFM, issue 1 (TN-SCIA-1000TP/194), Tech. rep., TPD, 1999. 1230

Edlou, S. M., Smajkiewicz, A., and Al-Jumaily, G. A.: Optical properties and environmental stability of oxide coatings deposited by reactive sputtering, Appl. Optics, 32, 5601–5605, doi:10.1364/AO.32.005601, 1993. 1229

Eplee Jr., R. E., Patt, F. S., Barnes, R. A., and McClain, C. R.: SeaWiFS long-term solar diffuser reflectance and sensor noise analyses, Appl. Optics, 46, 762–773, doi:10.1364/AO.46.000762, 2007. 1215

Fuqua, P. D., Morgan, B. A., Adams, P. M., and Meshishnek, M. J.: Optical Darkening During Space Environmental Effects Testing – Contaminant Film Analyses, Report TR-2004(8586)-1, Aerospace Corp, El Segundo, CA, 2004. 1215

Georgiev, G. T. and Butler, J. J.: Long-term calibration monitoring of Spectralon diffusers BRDF in the air-ultraviolet, Appl. Optics, 46, 7892–7899, doi:10.1364/AO.46.007892, 2007. 1215

Gottwald, M. and Bovensmann, H.: SCIAMACHY, Exploring the Changing Earth's Atmosphere, DLR, Dordrecht, NL, 2011. 1216, 1232

Gottwald, M., Krieg, E., Noël, S., Wuttke, M., and Bovensmann, H.: Sciamachy 4 years in orbit-instrument operations and in-flight performance status, in: Atmospheric Science Conference, Vol. 628 of ESA Special Publication, 2006. 1224

Green, D. B.: Satellite Contamination and Materials Outgassing Knowledgebase – an Interactive Database Reference, NASA STI/Recon Technical Report N, 1, 41072, 2001. 1215

Haynes, W. M. (Ed.): CRC Handbook of Chemistry and Physics, 93rd Edn. (internet version), CRC Press/Taylor and Francis, Boca Raton, FL, 2013. 1228

Hecht, E. and Zajac, A.: Optics, Addison-Wesley, Reading, MA, 1974. 1217

Jeurgens, L. P. H., Sloof, W. G., Tichelaar, F. D., and Mittemeijer, E. J.: Structure and morphology of aluminium-oxide films formed by thermal oxidation of aluminium, Thin Solid Films, 418, 89–101, 2002. 1225

Joos, F., Buenzli, E., Schmid, H. M., and Thalmann, C.: Reduction of polarimetric data using Mueller calculus applied to Nasmyth instruments, in: Observatory Operations: Strategies, Processes, and Systems II, edited by: Brissenden, R. J. and Silva, D. R., 70161I–70161I–11, 2008. 1225

Keller, C. U.: Instrumentation for astrophysical spectropolarimetry, in: Astrophysical Spectropolarimetry, edited by: Trujillo-Bueno, J., Moreno-Insertis, F., and Sánchez, F., 303–354, Cambridge University Press, Cambridge, UK, 2002. 1221, 1223

Krijger, J. M., Aben, I., and Schrijver, H.: Distinction between clouds and ice/snow covered surfaces in the identification of cloud-free observations using SCIAMACHY PMDs, Atmos. Chem. Phys., 5, 2729–2738, doi:10.5194/acp-5-2729-2005, 2005a. 1215

Krijger, J. M., Tanzi, C. P., Aben, I., and Paul, F.: Validation of GOME polarization measurements by method of limiting atmospheres, J. Geophys. Res.-Atmos., 110, D07305, doi:10.1029/2004JD005184, 2005b. 1214

Lang, R.: GOME-2/Metop-A Level 1B Product Validation Report No. 5: Status at Reprocessing G2RP-R2 v1F, Report EUM/OPS-EPS/REP/09/0619, EUMETSAT, 2012. 1216

Lei, N., Wang, Z., Guenther, B., Xiong, X., and Gleason, J.: Modeling the detector radiometric response gains of the Suomi NPP VIIRS reflective solar bands, in: Society of Photo-Optical Instrumentation Engineers (SPIE) Conference Series, Vol. 8533, doi:10.1117/12.974728, 2012. 1215, 1216

McMullin, D. R., Judge, D. L., Hilchenbach, M., Ipavich, F., Bochsler, P., Wurz, P., Burgi, A., Thompson, W. T., and Newmark, J. S.: In-flight Comparisons of Solar EUV Irradiance Measurements Provided by the CELIAS/SEM on SOHO, ISSI Scientific Reports Series, 2, 135, 2002. 1215

Meister, G. and Franz, B. A.: Adjustments to the MODIS Terra radiometric calibration and polarization sensitivity in the 2010 reprocessing, in: Society of Photo-Optical Instrumentation Engineers (SPIE) Conference Series, Vol. 8153, doi:10.1117/12.891787, 2011. 1215

Mott, N. F.: A theory of the formation of protective oxide films on metals, T. Faraday Soc., 35, 1175–1177, 1939. 1225

Noël, S., Bovensmann, H., Skupin, J., Wuttke, M. W., Burrows, J. P., Gottwald, M., and Krieg, E.: The SCIAMACHY calibration/monitoring concept and first results, Adv. Space Res., 32, 2123–2128, doi:10.1016/S0273-1177(03)90532-1, 2003. 1224

Palik, E. D. (Ed.): Handbook of Optical Constants of Solids, Vol. 1, Academic Press, New York, 1985. 1228

Rakic, A. D.: Algorithm for the determination of intrinsic optical constants of metal films: application to aluminum, Appl. Optics, 34, 4755–4767, doi:10.1364/AO.34.004755, 1995. 1228

Sankarasubramanian, K., Samson, J. P. A., and Venkatakrishnan, P.: Measurement of instrumental polarisation of the Kodaikanal Tunnel Tower Telescope, in: Solar Polarization: Proceedings of an International Workshop Held in Bangalore, India, 12–16 October 1998, edited by: Nagendra, K. N. and Stenflo, J. O., Kluwer Academic Publishers, 313–320, 1999. 1225

Schläppi, B., Altwegg, K., Balsiger, H., Hässig, M., Jäckel, A., Wurz, P., Fiethe, B., Rubin, M., Fuselier, S. A., Berthelier, J. J., De Keyser, J., Rème, H., and Mall, U.: Influence of spacecraft outgassing on the exploration of tenuous atmospheres with in situ mass spectrometry, J. Geophys. Res.-Space, 115, A12313, doi:10.1029/2010JA015734, 2010. 1215

5 Slijkhuis, S., Aberle, B., and Loyola, D.: Improvements of GDP Level 0–1 Processing System in the Framework of CHEOPS-GOME, in: Atmospheric Science Conference, Vol. 628 of ESA Special Publication, 2006. 1215

Snel, R.: In-orbit optical degradation: GOME experience and SCIAMACHY prediction, in: ERS-ENVISAT Symposium "Looking down to Earth in the New Millennium", CD-ROM, 2000. 1224

10 Stiegman, A. E., Bruegge, C. J., and Springsteen, A. W.: Ultraviolet stability and contamination analysis of Spectralon diffuse reflectance material, Opt. Eng., 32, 799–804, doi:10.1117/12.132374, 1993. 1215

Thiessen, G. and Broglia, P.: Uber einen Polarisationseffekt an aufgedampften Aluminiumschichten bei senkrechter Lichtinzidenz, Z. Astrophys., 48, p. 81, 1959. 1225

15 Tilstra, L. G., de Graaf, M., Aben, I., and Stammes, P.: In-flight degradation correction of SCIAMACHY UV reflectances and Absorbing Aerosol Index, J. Geophys. Res.-Atmos., 117, D06209, doi:10.1029/2011JD016957, 2012. 1214

van Harten, G., Snik, F., and Keller, C. U.: Polarization properties of real aluminum mirrors, I. Influence of the aluminum oxide layer, Publ. Astron. Soc. Pacific, 121, 377–383, doi:10.1086/599043, 2009. 1220, 1222, 1225, 1229, 1230

20 van Roermund, F.: SCIAMACHY Cleanliness and Contamination Control Plan, Report PL-SCIA-0000FO/05, BUPS, Delft, 1996. 1230

Xiong, X. X. and Barnes, W.: An overview of MODIS radiometric calibration and characterization, Adv. Atmos. Sci., 23, 69–79, doi:10.1007/s00376-006-0008-3, 2006. 1215

25 Xiong, X., Chiang, K., Esposito, J., Guenther, B., and Barnes, W.: MODIS on-orbit calibration and characterization, Metrologia, 40, S89, doi:10.1088/0026-1394/40/1/320, 2003. 1215
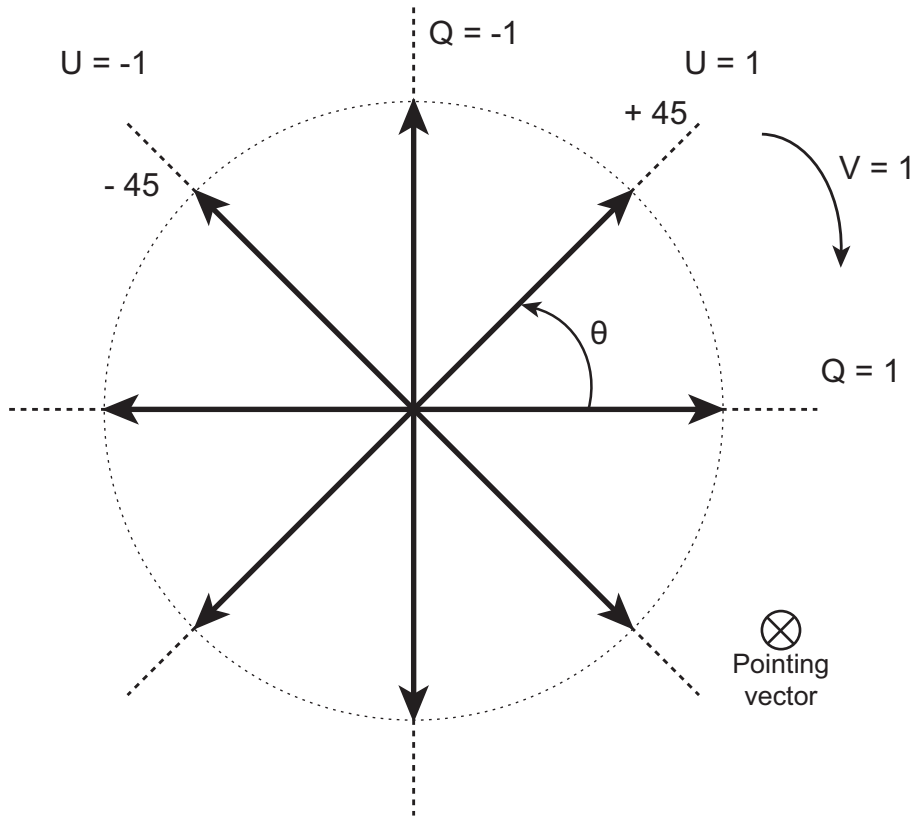
Fig. 1. Stokes vector frame definition used in the paper. Pointing vector is perpendicular and into the paper (following the light).
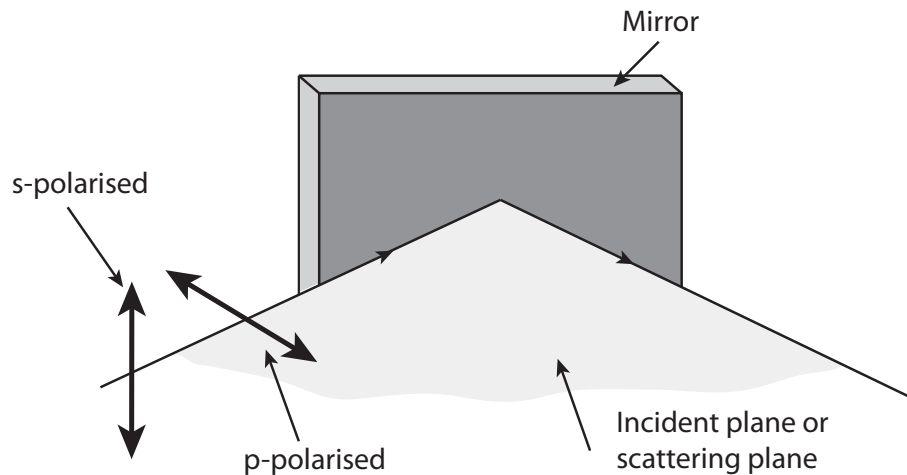
Full Screen / Esc

Printer-friendly Version

Interactive Discussion

Fig. 2. *s* and *p* polarisation direction definitions for a reflection.
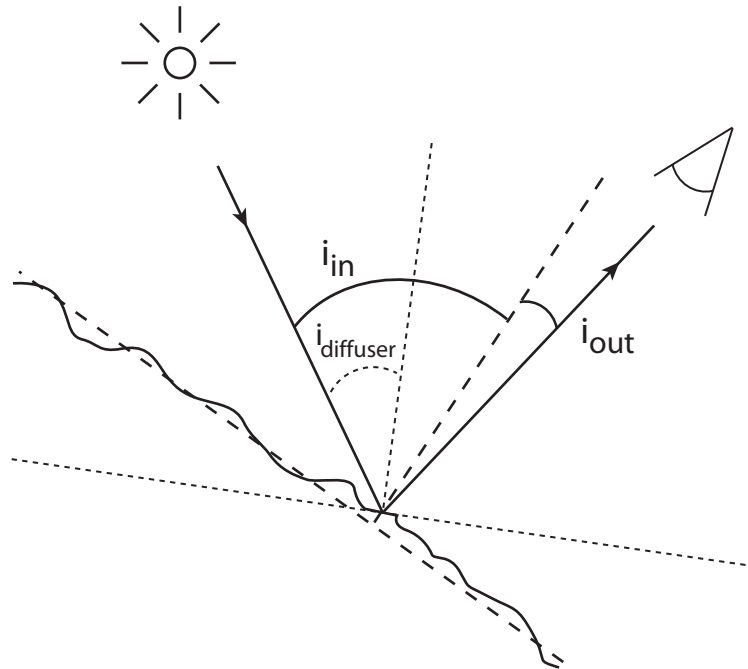
Fig. 3. Angle definitions used in mirror model for diffuser geometries. Solid curves with arrows indicate the light beam of interest with direction, long dashed curves indicate the macro-scale surface of the diffuser and its normal. Short dashed curves indicate the extrapolated surface and normal of the facet that causes the specular reflection of the lightbeam of interest. The various random (micro-scale) facets of the diffuser are indicated by the wiggly solid curve. Only facets oriented such that they cause specular reflection into the direction of the instrument contribute to the signal, dictating relative polarisation behaviour. Unpolarised reflectivity is only a function of the angular distribution of the facets of the diffuser, and the orientation of the diffuser in the light path.
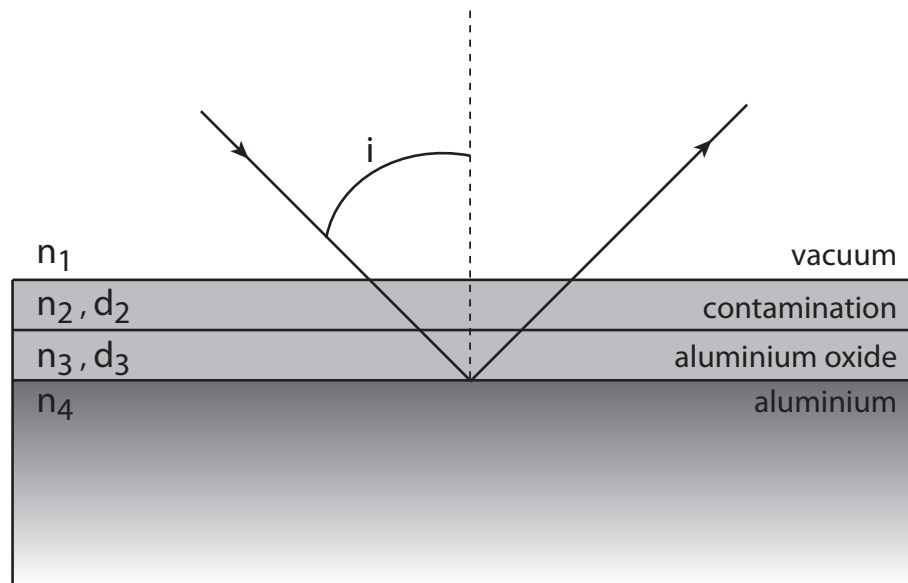
Fig. 4. Layers and angle definitions used in mirror model with thickness (d_i) and complex refractive index (n_i), left annotation for general case, right materials for SCIAMACHY application.
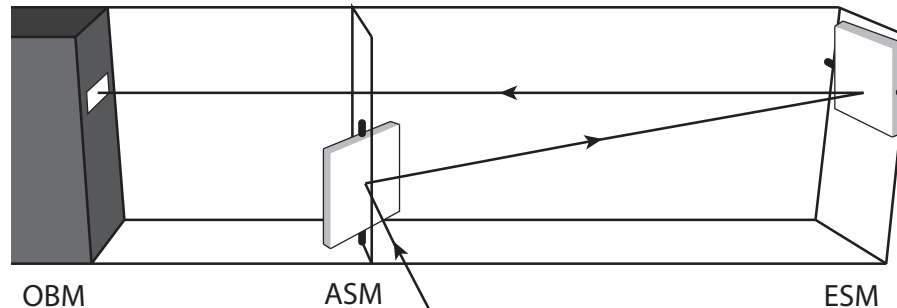
Fig. 5. Schematic view of SCIAMACHY multiple mirror setup in limb observation mode. On the left the Optical Bench Module (OBM) and entrance slit. On the right side the ESM, which if rotated to a 45° angle will reflect light (curve with arrow-head) coming from below (nadir) directly into the slit. In the middle the ASM which reflects the (limb) light coming from the front and slightly below, onto the ESM. Both mirrors have a bead-blasted aluminium surface diffuser on their backside (not shown here).
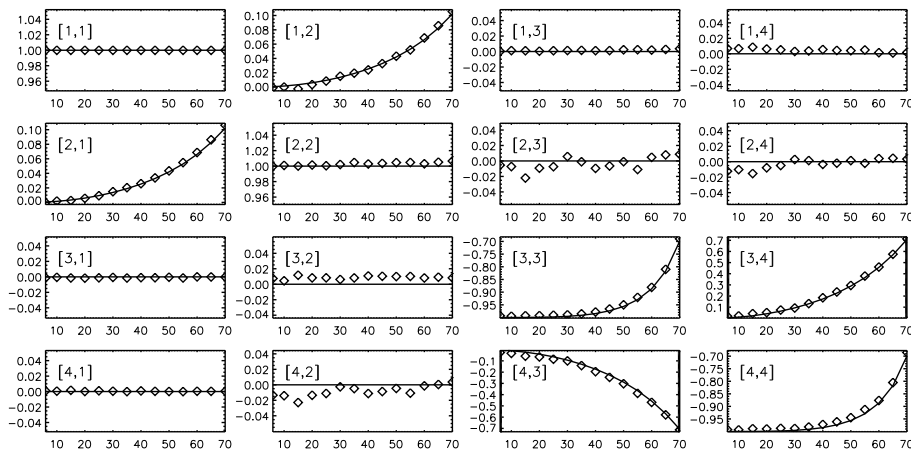
Fig. 6. Normalized Mueller matrix of reflection off a real aluminum mirror with an aluminum oxide layer of a measured 4.1 nm on top of it at 600 nm. Measurements by van Harten et al. (2009) (diamonds) and our model (lines).
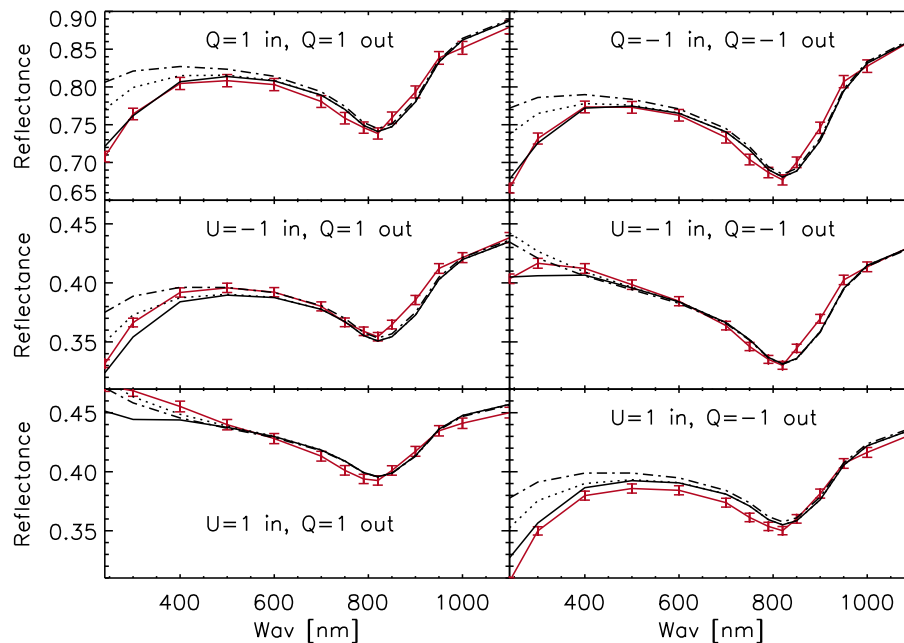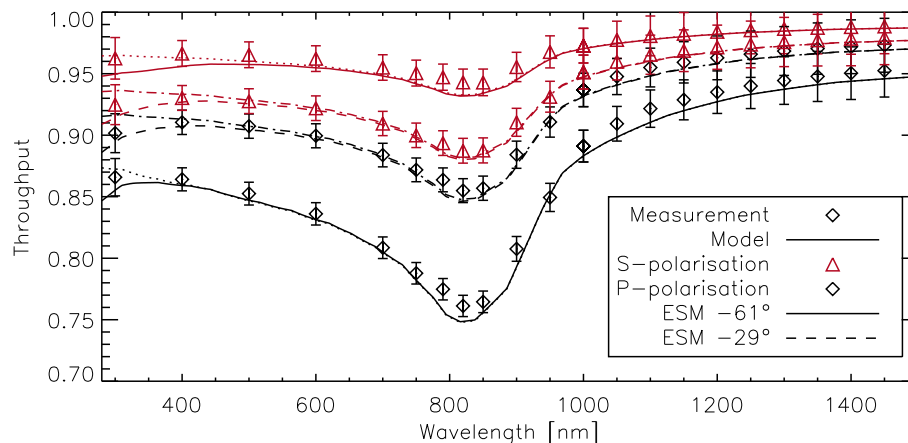
Fig. 7. SCIAMACHY scan mirror reflectance for different polarisation states of the incident light ($Q = 1$, $Q = -1$, $U = 1$, and $U = -1$ with respect to the SCIAMACHY reference frame) and different orientation of the analysers ($Q = 1$ and $Q = -1$), as indicated in the subplots. The measurement results with error bars obtained during on-ground calibration are shown in red, while the model calculations are represented by the black solid curve. The model calculation includes an aluminium mirror with 4.1 nm aluminium oxide and 0.4 nm of light oil contamination, and angles of incidence of $\phi_{ESM} = 12.7°$ and $\phi_{ASM} = 45°$. Dash-dotted curves indicate clean aluminium, and dotted curves aluminium with only 4.1 nm aluminium oxide, as comparison.

Title Page

Abstract | Introduction

Conclusions | References

Tables | Figures

Back | Close

Full Screen / Esc

Printer-friendly Version

Interactive Discussion

Fig. 8. SCIAMACHY scan mirror reflectance for different polarisation (S and P, i.e. $Q = 1$ and $Q = -1$) of the incident light and for different incident angles. Measurement during on-ground calibration are shown as diamonds. The curves represents the reflectance according to the mirror model, using an aluminium mirror with 4.1 nm aluminium oxide and 0.4 nm of light oil contamination, under an angle of incidence of either 29° (dashed) or 61° (solid). Dotted and dash-dotted curves indicate reflectance of clean aluminium instead as comparison.

Title Page

Abstract | Introduction

Conclusions | References

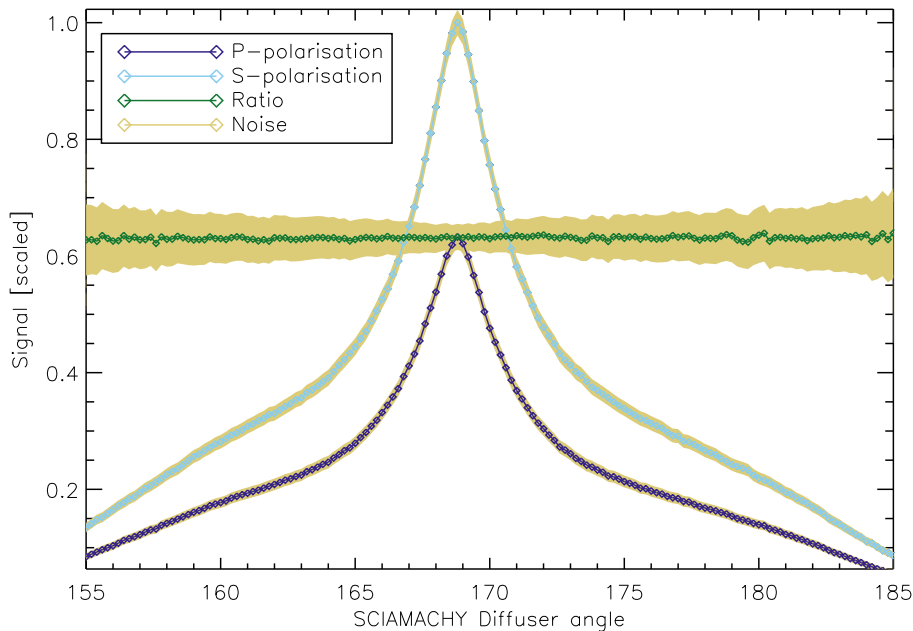Tables | Figures

◄ | ►

◄ | ►

Back | Close

Full Screen / Esc

Printer-friendly Version

Interactive Discussion

Fig. 9. Diffuser Model verification: scaled measured SCIAMACHY signal of the main science detectors as function of commanded diffuser angle for both s ($Q = 1$) and p polarisation ($Q = -1$) at 324 nm. Estimated uncertainties or noise (1σ) are indicated by the filled yellow areas. As expected the ratio between s and p polarisation (green curve) does not change as function of the diffuser angle.

Title Page

Abstract | Introduction

Conclusions | References

Tables | Figures

|◄ | ►|

◄ | ►

Back | Close

Full Screen / Esc

Printer-friendly Version

Interactive Discussion